Appendix A

U-shaped sample measurements

In this Appendix preliminary EE measurements conducted on a different sample, and with a different setup will be presented. The reason why these have been placed in the Appendix rather than in the main body resides in the preliminary nature of these measurements, conducted only for one value of current and magnetic field, and not supported by experiments on the magnetic structure of the sample employed, like it has been done for Sample 1 and 2. The first section will concern the new sample utilised, describing the microfabrication process, and the issues associated to it. Successively the new setup will be described, and the results presented, together with a short discussion.

A.1 Sample 4

The results obtained for the thermomagnetic characterization of the Hall bars (Sample 1 and 2) have been described in the main body, together with the issues associated to those measurements. To try and obtain different temperature gradient contributions in the same device, as done by Uchida [A1], a U-shaped device was fabricated, starting from the film with the capping layer (Sample 3). This U-shaped sample will hereafter be labeled Sample 4. Pictures of the pattern printed on the sample are showed in Figure A.1, with a close-up on the U-shaped device in Figure A.1b. The set of 8 patterns depicted in Figure A.1a has been repeated 16 times across the whole film. The length of the three segments of the U is 20 μm, with a width of 3 μm. The rest of the pattern, composed of the two large triangles behind the U, is needed to wire-bond the connections to the PCB. In this case, indeed, gold contacts have not been deposited due to an issue that will be discussed further, therefore the wire-bonds have been applied directly to the material.

As for the previous patternings, also in this case, the film has been sent to imec for patterning, but the mask design has been created in-house. In addition, electron beam lithography (EBL) has been employed in place of photolithography, due to the specificity of the patterns to print. However, the employment of EBL led to an issue which was avoided in the previous cases: for this technique, the most used resist is PMMA (Polymethyl methacrylate), which is a positive resist, therefore it is removed where exposed. Unfortunately the successive ion milling performed to remove CMG in the non-desired locations crosslinked PMMA and turned into a negative resist. This was the issue mentioned before, as crosslinked PMMA is notoriously hard to remove [A2, A3, A4]: for this reason, gold contacts were not deposited, and it was not possible to carry out measurements until the polymer was stripped off, at least locally on the U pattern.

The first attempt was to immerse the sample in hot acetone at 60° overnight: the results are visible in Figure A.2a, clearly indicating that the polymer is still attached in proximity

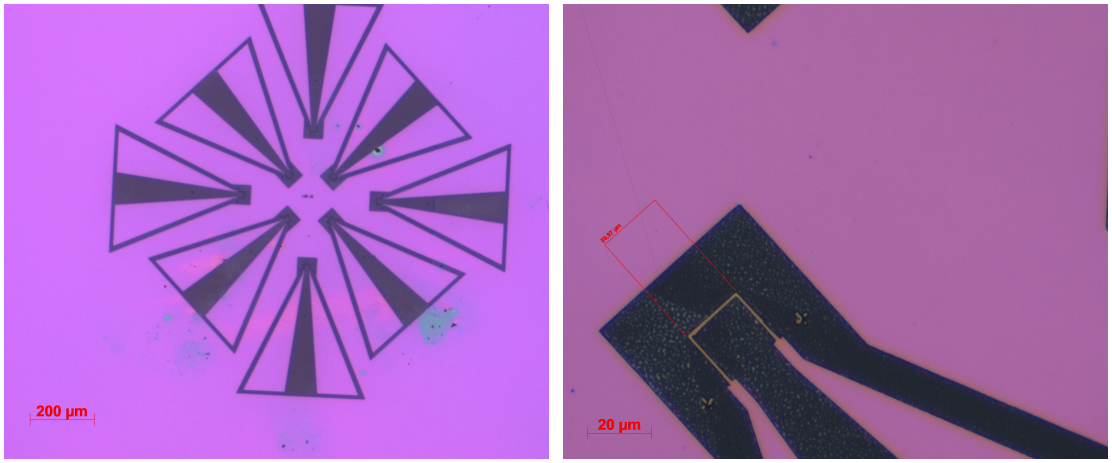

(a) (b)

Figure A.1: Optical microscope images of a) a set of patterns printed on the sample and b) a close-up of the U pattern, with the length of the central leg.

of the patterns. Therefore, a stronger solvent (DMSO, dimethylsulfoxide) was employed, immersing the sample in a hot bath of DMSO for 10 hours. However, also this attempt was unsuccessful, removing part of the crosslinked PMMA, but not completely (Figure A.2b). From here, two different strategies were followed: the first one consisted in mechanical cleaning of the U pattern with contact AFM, scratching off the polymer, whereas the second employed sonication of the sample for 15 seconds. The results for the former strategy are displayed in Figure A.3a: after many repeated scans, the polymer was indeed scratched off. With sonication (Figure A.3b) the obtained image was not as clear and tidy as the one obtained after AFM cleaning. However, mechanical AFM cleaning is very time consuming, as many repeated scans are required to clean just one pattern, whereas, being sonication much more time effective, this was chosen as the cleaning method. The devices cleaned by sonication are therefore the ones on which the measurement has been performed. After the cleaning, the sample has been wire-bonded attaching the wires at the bottom of the two triangular patterns visible in Figure A.1a: in this case, possible residues of PMMA do not constitute an issue, as the wire-bonds penetrate through the polymer, landing on the sample.

For this sample, the OOP hysteresis should be roughly the same as the one showed in section 2.4: also Sample 4 indeed originates from the film with the capping layer characterised at KUL. The shape is different, but being both thin films, this should not radically change the hysteresis cycle. However, as it will be presented in the next section, for this measurement the magnetic field will be applied IP: for this orientation, experimental hysteresis cycles are not available yet, therefore one has to rely on literature sources.

A.2 Setup

As discussed in the main body, the limitations in the setup employed led to the adoption of OOP magnetic field for the first experiments. Owing to the high field needed to saturate the sample (1 T), the sample was never brought to saturation during the experiments, as the maximum achievable OOP field with our setup was 700 mT. This could have limited the magnitude of the EE, as it scales with the magnetization of the sample. For this reason,

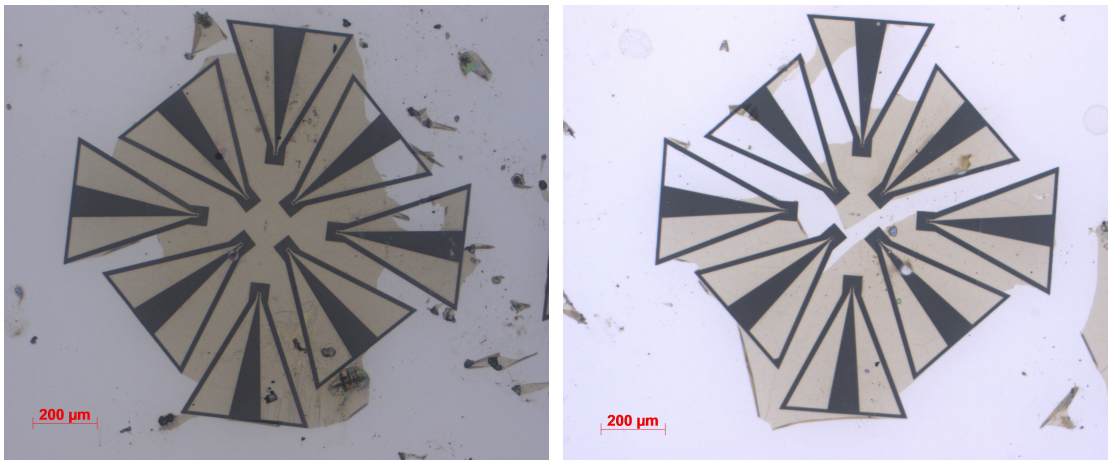

(a) (b)

Figure A.2: Microscope images of the printed patterns after a bath of a) hot acetone overnight, and b) hot DMSO for 10 h. The yellowish coating is the PMMA, the white substrate the capping layer, and the black regions are the printed pattern.

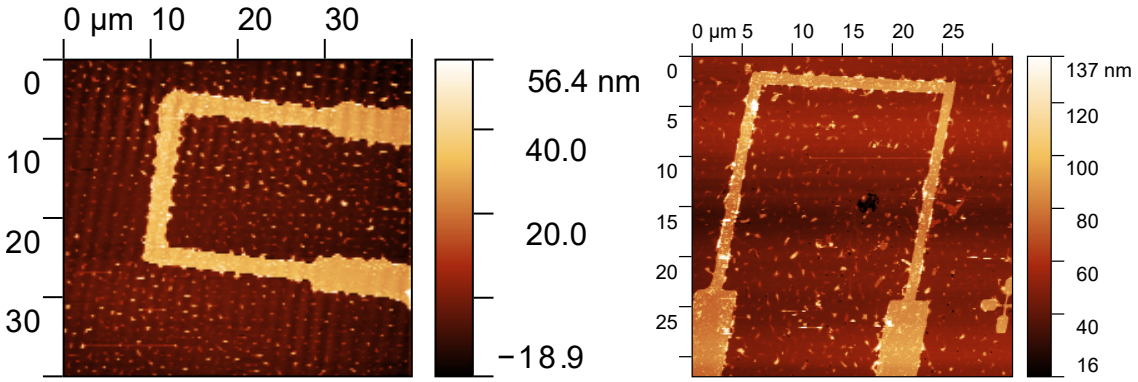

(a) (b)

Figure A.3: AFM topographic maps of the pattern a) after mechanical cleaning by AFM, and b) after sonication. The scan angle has been rotated by 90° between the two scans.

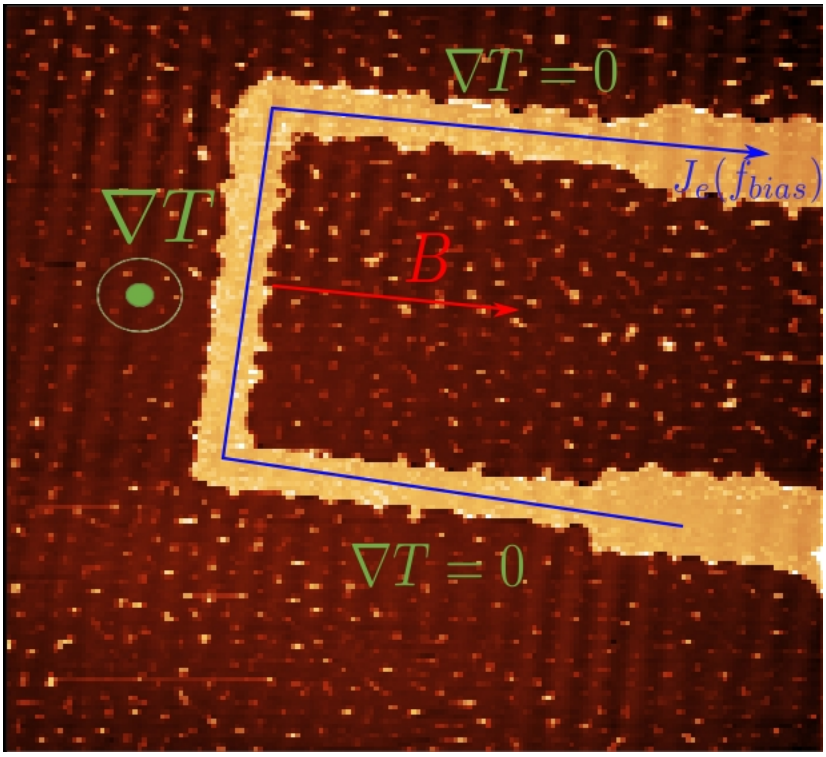

Figure A.4: AFM topographic map modified to show the direction of the current, magnetic field and temperature gradient (respectively in blue, red and green) in the different parts of the U pattern.

the most suitable configuration to investigate EE requires the magnetic field to be IP, since in this case, the sample is saturated with 25 mT [A5], as showed in Figure 3.16a, and it is easier to saturate the sample, aiming for the maximum amplitude of the effect.

The principle is therefore to employ the fact that the current is forced to flow in different direction within the U pattern. Applying an IP magnetic field which is perpendicular to the central leg of the pattern (as in Figure A.4) generates an OOP temperature gradient, whereas the two parallel legs of the U pattern give no signal, since the magnetic field will be parallel to the current. The EE, therefore, should be visible only in the central part of the leg, which should allow for an easier visualization in the maps. The expected features therefore correspond to a uniform signal in the central part of the U pattern either in the amplitude and phase map, since in this case the temperature gradient develops across the 50 nm thick film, but the scan probes only the top surface.

To generate an IP magnetic field, two rectangular magnets have been employed: the purpose of this arrangement was to build a first proof of concept setup able to produce an IP field, without being necessarily able to tune its magnitude. This would be the objective for the next steps to carry out within this project. The magnets setup, sketched in Figure A.5a, is comprised of two rectangular magnets of dimensions 2 x 2 x 3 cm^3, between which a Kapla wooden block has been sandwiched, acting as a spacer. The width of this block is 0.8 cm: its purpose is to separate the two magnets, so that the field lines bulge on top of the surface (as it is showed in Figure A.5a) and it is possible to place the PCB on top of the setup, producing a field larger anyway than the saturation one. Placing the sample exactly aligned at the center of the magnets setup, the IP fields results to be 170 mT, after measurements with a gaussmeter: as the sample is moved off-axis and far from the center,

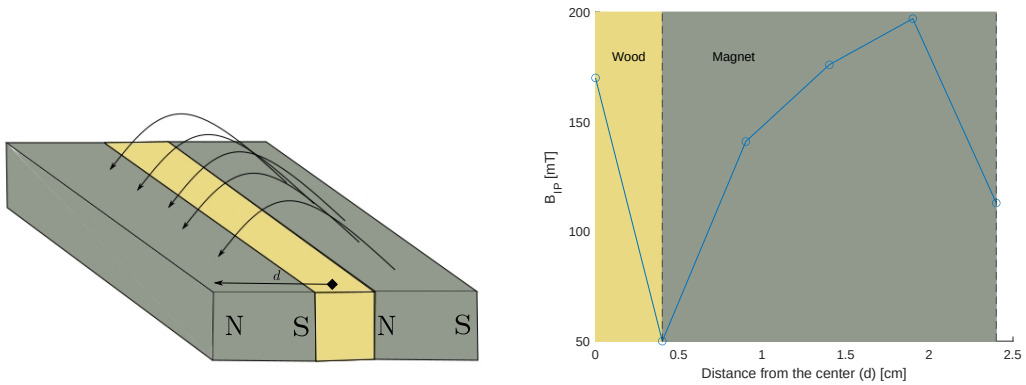

(a) (b)

Figure A.5: a): Sketch of the setup employed to generate IP magnetic field: the grey rectangles represent the magnets, with their pole orientation, the yellow block is the wooden block. Also the direction along which the field has been plotted (d) is represented. b): Calibration curve of the magnets setup: magnetic field on top of the structure against distance from the center of the wooden block. A division between the wooden block and the magnet has been included.

the field decreases as showed in Figure A.5b. The field drops at the interface wood-magnet: on top of the magnet it is even stronger than in the center, probably owing to the field lines closing on the other pole. A possible improvement could be indeed positioning the sample on top of the magnet, where the gradient of the field is lower than at the center, so that even if the sample is not completely aligned, the field will be approximately in the same range.

The rest of the experimental setup is the same as the one described in section 3.2: the same instruments have been employed, with the same connections as the ones already described. The magnets setup has been placed on top of a iron block of height 2 cm, and 10 x 5 cm^2 length and width. Indeed, the AFM employed has itself magnetic parts that could have attracted the magnets when the tip is brought into contact. Sticking the iron block on the magnetic plate of the instrument, and the magnets on top of that, ensures enough attractive force to keep the whole block in place even when the tip approaches the sample. The other experimental parameters have been kept equal to the ones employed in the experiments on Sample 1 and 2: the signal fed to the probe comprised again an AC component $V_{AC} = 4\,V$ peak to peak oscillating at 91 kHz, and a DC offset of $V_{DC} = 1\,V$. The frequency of the current has been kept at $f_{bias} = 17\ Hz$. In this case, the thermal time constant of the new device has not been simulated, but, being the same material, and considering that the temperature gradient will develop across a distance much smaller than the previous experiments (50 nm against 10 μm), one can expect a much smaller τ_s, meaning that the requirement $\omega\tau_s << 1$ will still hold with the same frequency as before. The resistance between the two wire-bonds has been measured ($R = 1.75\,k\Omega$) in order to input the voltage correspondent to the desired current. The amplitude of the current has been decreased to $50\,\mu A$: being the sample narrower, this smaller current produces a current density $J_e = 3.33 * 10^8 A/m^2$, which is in the same range as the ones employed previously. Employing higher currents would have led to even higher current densities, taking the risk of damaging the sample. The scan rate has been kept to 0.1 Hz, the value

identified in section 3.2 as the minimum one required to allow thermalization of the tip at each point.

A.3 Results

The following maps have therefore been obtained for a field of $B = 170\,mT$ and a current of $I = 50\,\mu A$. The whole U pattern is clearly visible in the three maps displayed in Figure A.6, and some residues of polymer can be spotted as well. Also the phase map at the first harmonic has been obtained, but it displayed a linearly periodic signal which cannot be correlated to the device scanned, therefore it has not been showed. What strikes the eye is that the two amplitude maps, at the first and second harmonic, are rather similar. In particular, many features which are visible in the topography map appear in the two amplitude maps, suggesting that in both cases the SThM signal was deeply affected by the topography of the sample. This is probably linked to the incomplete cleaning of the device: many spots are visible in the maps, and, as discussed in the main body, thickness variations strongly affect the signal coming from the SThM, imaging the same topography features due to different heat transmission. The Pearson number, indeed, between the two amplitude maps and the topography one is higher than the one computed for the experiments on Sample 1 and 2. Whereas in those cases, the coefficient was smaller than 0.1, it took on a value of 0.28 for the first harmonic map, and 0.3 for the second harmonic one, signaling a stronger correlation than in the previous cases.

For future experiments, it would be beneficial to i) achieve a better cleaning of the sample, in order to minimize the topography features in the amplitude maps and ii) increase the current injected in the sample. Indeed, employing the relationship between the generated temperature difference and the input current and field, it is easy to find that the output is independent of the thickness of the sample, and depends linearly on the current. Indeed:

$$\nabla T = \frac{P_{EE} B I}{t w}, \tag{A.1}$$

$$\Delta T = \frac{P_{EE} B I}{w}, \tag{A.2}$$

with t thickness of the sample, w its width, ΔT temperature difference, ∇T temperature gradient, and $\nabla T = \Delta T / t$, since the temperature gradient develops across the thickness of the sample. What this means is that, with respect to the OOP magnetic field configuration, the beneficial effect of employing an IP field and easily saturating the sample is counterbalanced by a smaller expected temperature difference. Indeed, for the previous configuration, Equation A.1 remains unaltered, but, in that case, $\nabla T = \Delta T / w$, bringing a term t to the denominator of Equation A.2. Being the thickness much smaller than the width of Sample 4 (50 nm vs 3 μm), the expected ΔT is much higher in the first case. Larger currents could therefore be beneficial, even if, again, the reduced width poses some limitations in terms of current density. Injecting a current of 1 mA into Sample 4, as it has been done in the previous experiments, indeed, would lead to a density current of $7{*}10^{10}$ A/m^2, larger than the ones used in other experiments on CMG [A6, A7], and taking the risk of damaging the sample.

The previous reasoning made analysing the two equations Equation A.1 and A.2 is confirmed by the graph of Figure A.7, which shows that, in a range of current going from 50 μA (the current used in the experiment) to 5 mA the obtained temperature difference is always below the resolution limit, set at 0.1 K. In this case, experimental hysteresis curves for IP magnetic field were not available, so the value of saturation magnetization was taken

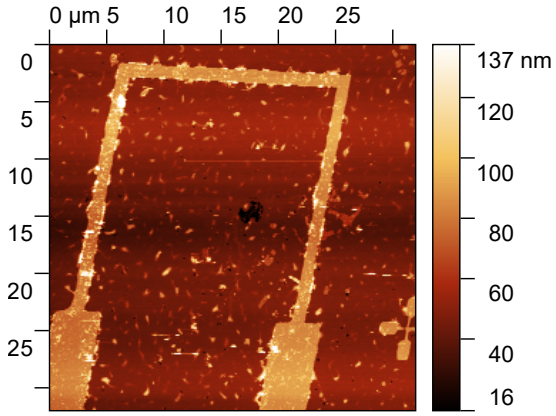

(a) Topography map

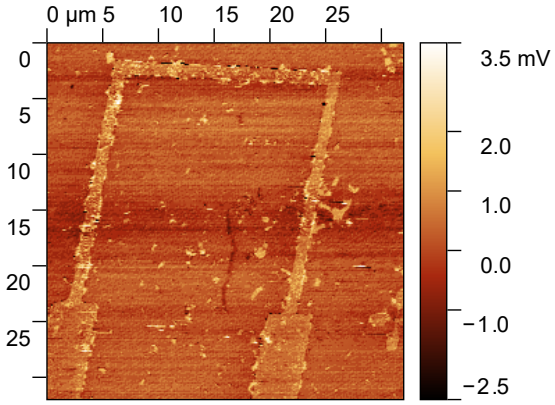

(b) Amplitude map at f_{bias}

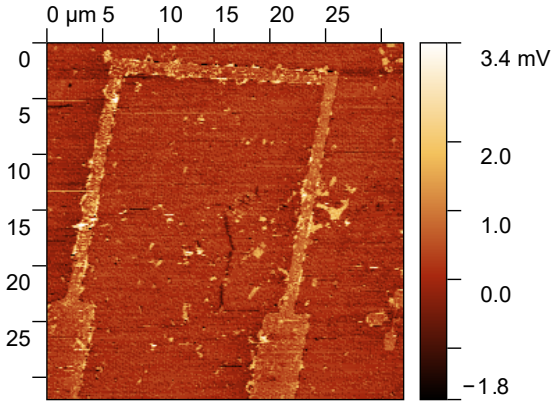

(c) Amplitude map at $2f_{bias}$

Figure A.6: Thermomagnetic characterization of Sample 4 at $B = 250\,mT$ IP, and $I = 50\,\mu A$: the topography, amplitude at the first and second harmonic are showed.

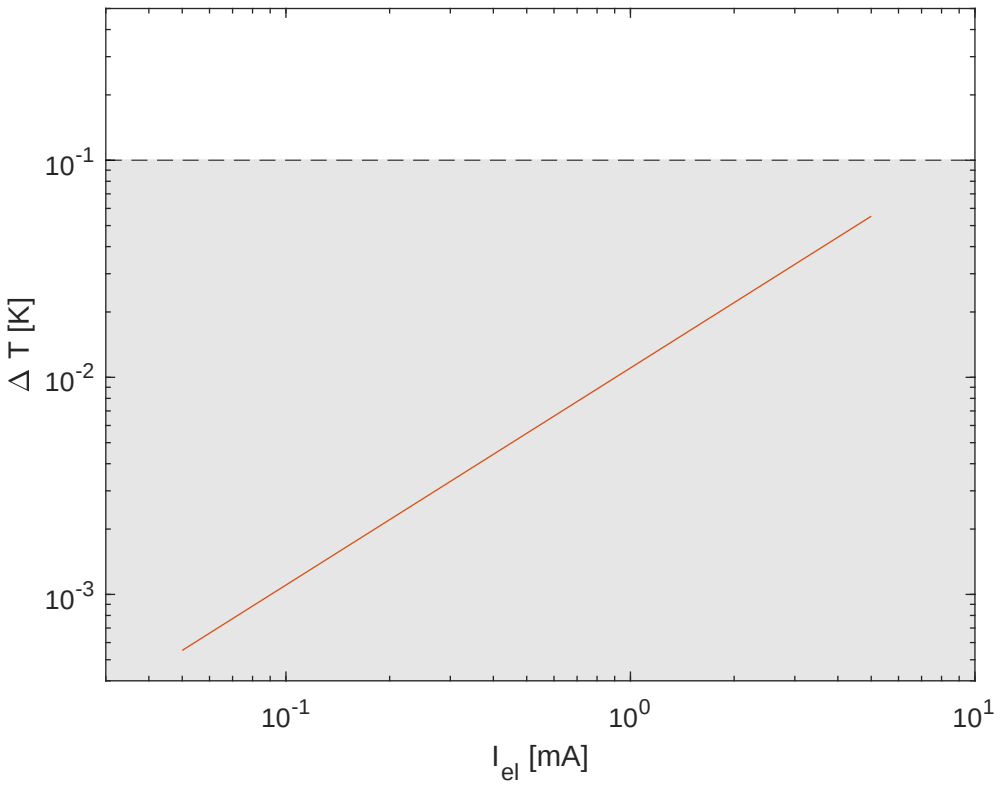

Figure A.7: EE-induced temperature difference obtained from the Bridgman relation in Sample 4 against injected electric current in the device, with an IP field of 170 mT. The grey area corresponds to the temperature difference below the resolution limit of 0.1 K.

from literature ([A5]), being 600 emu/cm^3. This graph confirms that the detrimental effect of developing a temperature gradient across the thickness rather than across the much larger width, completely outweighs the benefit of bringing the sample to saturation with the IP field. In light of this conclusion, the best strategy to increase the signal is probably to saturate the sample OOP with a larger field, in order to bring anyway the material to saturation, and retaining a gradient developing across the width. Indeed, even with a current of 5 mA, which, as explained before, could damage the sample, the effect would still be in the range of mK, too weak to be picked up.

Appendix bibliography

[A1] Ken-Ichi Uchida, Shunsuke Daimon, et al. Observation of anisotropic magneto-Peltier effect in Nickel. Nature, 558, 2018.

[A2] I Zailer, J E F Frost, et al. Crosslinked PMMA as a high-resolution negative resist for electron beam lithography and applications for physics of low-dimensional structures. Semiconductor Science and Technology, 11, 1996.

[A3] Faiz Rahman, Daniel J. Carbaugh, et al. A review of polymethyl methacrylate (PMMA) as a versatile lithographic resist – With emphasis on UV exposure. Microelectronic Engineering, 224, 2020.

[A4] Daniel J. Carbaugh, Sneha G. Pandya, et al. Enhancing the dry etch resistance of polymethyl methacrylate patterned with electron beam lithography. Journal of Vacuum Science Technology B, 35(4), 2017.

[A5] Yao Zhang, Yuefeng Yin, et al. Berry curvature origin of the thickness-dependent anomalous Hall effect in a ferromagnetic Weyl semimetal. npj Quantum Materials, 6, 2021.

[A6] Taqiyyah S. Safi, Chung-Tao Chou, et al. Spin-generation in magnetic Weyl semimetal Co2MnGa across varying degree of chemical order. Applied Physics Letters, 121, 2022.

[A7] Ke Tang, Zhenchao Wen, et al. Magnetization switching induced by spin–orbit torque from Co2MnGa magnetic Weyl semimetal thin films. Applied Physics Letters, 118, 2021.